Naphthyl Radical: Negative Ion Photoelectron Spectroscopy, Franck−Condon Simulation, and Thermochemistry

ARTICLE *in* THE JOURNAL OF PHYSICAL CHEMISTRY A · NOVEMBER 2001

Impact Factor: 2.69 · DOI: 10.1021/jp011779h

Naphthyl Radical: Negative Ion Photoelectron Spectroscopy, Franck−Condon Simulation, and Thermochemistry

Kent M. Ervin,*,† Tanya M. Ramond,‡ Gustavo E. Davico,‡,§ Rebecca L. Schwartz,‡,|| Sean M. Casey,† and W. Carl Lineberger*,‡

JILA, University of Colorado and National Institute of Standards and Technology, and Department of Chemistry and Biochemistry, University of Colorado, Boulder, Colorado 80309-0440; and Department of Chemistry and Chemical Physics Program, University of Nevada, Reno, Nevada 89557

Received: May 9, 2001; In Final Form: October 1, 2001

The naphthyl anion ($C_{10}H_7^-$, naphthalenide) is prepared in a flow tube reactor by proton transfer between NH_2^- and naphthalene ($C_{10}H_8$). The photoelectron spectrum of this anion is measured at a fixed laser wavelength of 364 nm. A single electronic band is observed, corresponding to the neutral naphthyl radical ($C_{10}H_7$, naphthalenyl). The Franck−Condon profiles for both 1-naphthyl (α-naphthyl) and 2-naphthyl (*β*-naphthyl) are simulated on the basis of density functional theory calculations of the vibrational frequencies and normal coordinates. Issues involving Franck−Condon simulations for large polyatomic molecules and Duschinsky rotation are discussed, and improved Franck−Condon simulation algorithms are presented. Comparison of the Franck−Condon simulations with the photoelectron spectrum shows that the observed band is predominantly due to the 1-naphthyl isomer, consistent with previous measurements showing the 1-naphthyl anion as more stable than the 2-naphthyl anion. The observed electron affinity of the 1-naphthyl radical is $EA_0(1\text{-}C_{10}H_7) = 1.403 \pm 0.015$ eV. On the basis of an evaluation of literature data, the recommended gas-phase acidity of naphthalene is $\Delta_{acid}H_{298}(1\text{-}C_{10}H_7\text{−H}) = 1649 \pm 14$ kJ/mol and the recommended bond dissociation energy of naphthalene is $DH_{298}(1\text{-}C_{10}H_7\text{−H}) = 472 \pm 14$ kJ/mol.

Introduction

Polycyclic aromatic hydrocarbons (PAHs) are of interest because of their role in combustion,[1,2] their possible presence in interstellar environments,[3] and their carcinogenic properties.[4] The radicals of PAHs are reaction intermediates in various combustion processes leading to fullerene and soot formation.[5,6] For these reasons, the CH bond dissociation energies of benzene[7] and polycyclic aromatic hydrocarbons[2,8−10] have been recent targets of experimental and theoretical study.

Gas-phase ion chemistry and mass spectrometry provide valuable methods for determination of thermochemical stabilities of neutral hydrocarbon radicals.[11,12] The negative ion thermochemical cycle given by eq 1 relates the C−H bond dissociation energies of a neutral hydrocarbon to its gas-phase acidity and the electron affinity of the radical.

$$D(\text{R−H}) = \Delta_{acid}H(\text{RH}) + \text{EA(R)} - \text{IE(H)} \qquad (1)$$

Here we measure the electron affinity of naphthyl radical, $C_{10}H_7$, using negative ion photoelectron spectroscopy and we reevaluate the gas-phase acidity and the CH bond dissociation energy of naphthalene, $C_{10}H_8$.

Previous values of the gas-phase acidity of naphthalene and the electron affinity of naphthyl radical are shown in Table 1. Meot-Ner et al.[13] used proton-transfer equilibrium studies with high-pressure mass spectrometry (HPMS) to measure the gas-phase acidity of naphthalene. Two isomers can be formed upon deprotonation, either 1-naphthyl (α) or 2-naphthyl (*β*) anions. Meot-Ner et al. predicted on the basis of AM1 calculations that $1\text{-}C_{10}H_7^-$ is more stable. The relative gas-phase acidities of naphthalene to form 1-naphthyl and 2-naphthyl anions and the relative electron affinities of the 1-naphthyl and 2−naphthyl radicals have been reported recently, using kinetic correlation methods.[8,9] Reed and Kass[8] used ion cyclotron resonance (ICR) mass spectrometry with the DePuy silane cleavage kinetics method[14,15] to estimate the relative proton affinities of 1-naphthyl and 2-naphthyl anions, using methane, ethane, cyclopropane, ethene, and benzene as calibration acids. The 1- and 2-trimethylsilylnaphthalenes were synthesized to obtain selective acidities for each deprotonation site, via the competitive reaction with OH^- to form naphthalene or methane. Their work confirms that removal of the proton from naphthalene at the α position to form the $1\text{-}C_{10}H_7^-$ anion is favored (smaller value of $\Delta_{acid}H$) over proton removal from the *β* position to form the $2\text{-}C_{10}H_7^-$ anion (Table 1). Reed and Kass[8] also obtained the electron affinities of 1-naphthyl and 2-naphthyl radicals using the single-reference version[16] of the Cooks kinetic method,[17,18] with SO_2^- as the reference anion and phenyl, *m*-benzyne, and *o*-benzyne anions as calibration species. The logarithm of the ion ratio for competitive formation of R^- and SO_2^- in collision−induced dissociation of the $(R\cdot SO_2)^-$ complex is correlated with EA(R)-EA(SO_2). The complex of SO_2 with 1- or 2-naphthyl anion is produced by the reactions of F^- with 1- or 2-trimethylsilylnaphthalene to form the anion followed by termolecular association with SO_2. Reed and Kass find that $1\text{-}C_{10}H_7^-$ is more stable than $2\text{-}C_{10}H_7^-$ relative to the corresponding neutral

* Authors to whom correspondence should be addressed. E-mail: ervin@chem.unr.edu (K. M. Ervin); wcl@jila.colorado.edu (W. C. Lineberger).
† University of Nevada.
‡ University of Colorado.
§ Present address: Department of Chemistry, University of Idaho, Moscow, Idaho.
|| Present address: Federal Bureau of Investigation Laboratory, Quantico, Virginia.

10.1021/jp011779h CCC: $20.00
Published on Web 00/00/0000 PAGE EST: 9.3

TABLE 1: Thermochemistry of Naphthyl and Naphthalene

method	HPMS equilibrium (Meot-Ner et al.[13])	ICR kinetics (Reed & Kass[8])	QPMS kinetics (Lardin et al.[9])	this work
		Electron Affinities/eV		
$EA_0(1\text{-}C_{10}H_7)$		1.37 ± 0.02	1.43 ± 0.06	1.403 ± 0.015[a]
$EA_0(2\text{-}C_{10}H_7)$		1.30 ± 0.02	1.37 ± 0.04	$1.34^{+0.03}_{-0.07}$[b]
δEA_0		0.07 ± 0.03	0.06 ± 0.07	>0.05[c]
		Gas-Phase Acidities/kJ mol^{-1}		
$\Delta_{acid}H_{298}(1\text{-}C_{10}H_7\text{-H})$	1649 ± 5 (1642 ± 13)[d]	1656 ± 6[e]	1648 ± 20[e]	1649 ± 14[f]
$\Delta_{acid}H_{298}(2\text{-}C_{10}H_7\text{-H})$		1661 ± 5[e]	1664 ± 20[e]	1659 ± 20[g]
$\delta\Delta_{acid}H_{298}$		-5.4 ± 8	-15 ± 9	
		Bond Dissociation Enthalpies/kJ mol^{-1}		
$D_{298}(1\text{-}C_{10}H_7\text{-H})$		469 ± 5	474 ± 22	472 ± 14[h]
$D_{298}(2\text{-}C_{10}H_7\text{-H})$		468 ± 5	483 ± 21	476 ± 20[h]
δD_{298}		-1.4 ± 9	9.2 ± 11	

[a] Measured electron affinity from photoelectron spectrum. [b] Calculated from $EA_0(1\text{-}C_{10}H_7)$ using average relative value δEA from the kinetics experiments. [c] Limit based on Franck−Condon simulations, see text. [d] Reevaluated from data of Meot-Ner et al., see text. [e] Directly measured values, not calibrated to equilibrium value. [f] Recommend value based on average of previous literature results. [g] Calculated from $\Delta_{acid}H_{298}(1\text{-}C_{10}H_7\text{-H})$ using average relative value of $\delta\Delta_{acid}H_{298}$ from the kinetics experiments. [h] Calculated using eq 1.

radicals (larger electron affinity for $1\text{-}C_{10}H_7$, Table 1). More recently, Lardin et al.[9] applied the same kinetic correlation methods for the determination of the naphthalene gas-phase acidities and naphthyl electron affinities. They employed a flowing afterglow/triple quadrupole mass spectrometer (QPMS) instrument with variable collision energy and they used different sets of calibration compounds (methane, benzene, and propylene for the gas-phase acidities and *p*-benzyne, phenyl, *p*-chlorophynl, *m*-bromobenzyl, *p*-bromobenyzl, *m*-chlorobenzyl, and *p*-chlorobenzyl anions for the electron affinities). They also used a version of the Cooks kinetic method that includes an analysis of entropy effects.[9,19,20] As shown in Table 1, the primary results of the two experiments showing that the 1-naphthyl anion is slightly more stable than the 2-naphthyl anion are in good accord.[8,9] Using eq 1, these kinetic results imply that the difference between the bond dissociation energies for removal of H from naphthalene at the two possible sites, $\delta D_{298} = D_{298}(1\text{-}C_{10}H_7\text{-H}) - D_{298}(2\text{-}C_{10}H_7\text{-H})$, is smaller than the uncertainties.

The kinetic correlation methods used by these previous studies[8,9] should give reasonable estimates of the *relative* gas-phase acidities and electron affinities of the two naphthyl isomers. Both kinetic methods rely on the competition between two product channels from an intermediate or complex, with the two rates being correlated with the thermochemical stability of the products. Kinetic method results are affected by the complexation energy, the size of the complexes, the experimental energy distributions, and the intrinsic nature of the transition states.[11,18,21−23] Because the two naphthyl isomers have very similar electronic and geometric structures in both the anion and neutral states, these kinetic factors controlling the decomposition of intermediates, namely the well depths and dissociation transition states, should be very similar so that the relative dissociation rates are mainly controlled by the differences in the energies rather than entropic factors. Because the calibration compounds are less similar to naphthalene, however, and because the correlations involve extrapolations outside the range of electron affinities and gas-phase acidities of the parent calibration compounds, the *absolute* thermochemical values obtained by the kinetic correlation methods are less certain. It is encouraging that the two ion kinetics experiments using different instrumentation give similar results.[8,9] Nevertheless, it is useful to obtain an independent absolute measurement of the electron affinity of naphthyl, a primary goal of this work.

Photoelectron Spectroscopy Experiment

The experiments are conducted using a negative ion photoelectron spectrometer that has been described in detail previously.[24−26] The negative ion source is a microwave discharge in a flowing afterglow flow tube reactor operating at 0.36−0.44 Torr of helium buffer gas and a nominal temperature of 300 K. Ions are extracted from the flow tube through an aperture, focused into an ion beam and accelerated to 735 eV, mass selected with a Wien velocity filter, and then decelerated to 40 eV in the interaction region. There the ions are crossed by a continuous laser beam at a wavelength of 364 nm (3.408 eV photon energy) from an argon ion laser, which is amplified in an external power build-up cavity.[25] The kinetic energies of the photodetached electrons are measured with a hemispherical electrostatic electron energy analyzer coupled with a position-sensitive detector.[24] The absolute energy scale of the spectrometer is calibrated with O^- and NH_2^- using the known values[27−30] of $EA(O) = 1.4611100 \pm 0.0000007$ eV and $EA(NH_2) = 0.771 \pm 0.005$ eV. A small linear correction (0.24% in this work) that accounts for an energy scale compression of the hemispherical analyzer is determined from the fine structure splittings of tungsten atoms in the photoelectron spectrum of W^-. The instrumental resolution of 10−15 meV (full-width at half-maximum) is determined from O^- and NH_2^- calibration spectra taken during each experimental session. All spectra are taken with the laser polarization at the magic angle of 54.7° relative to the direction of photoelectron detection, giving intensities proportional to the total photodetachment cross section.

In this work, naphthyl anions ($C_{10}H_7^-$) are produced by reaction 2 in the flowing afterglow source.

$$NH_2^- + C_{10}H_8 \rightarrow NH_3 + C_{10}H_7^- \qquad (2)$$

Use of O^- or OH^- as precursor ions did not give sufficient intensities of $C_{10}H_7^-$. Amide anions (NH_2^-) are produced by adding ammonia gas as precursor upstream of the microwave discharge. Naphthalene vapor from a gently heated sample of the solid is introduced into the flow tube downstream of the discharge. Because both NH_2^- and $C_{10}H_7^-$ are strong bases, they react exothermically by proton transfer with water impurities in the flow tube. Obtaining high intensities of NH_2^- required using high-purity helium (Spectra Gases, 99.9999%) for the flow tube buffer gas. Reaction 2 is sufficiently exergonic,[31] $\Delta_rG_{298} = -54 \pm 5$ kJ/mol, that this reaction is irreversible under the flow tube conditions. In the kinetic limit where reaction 2 does

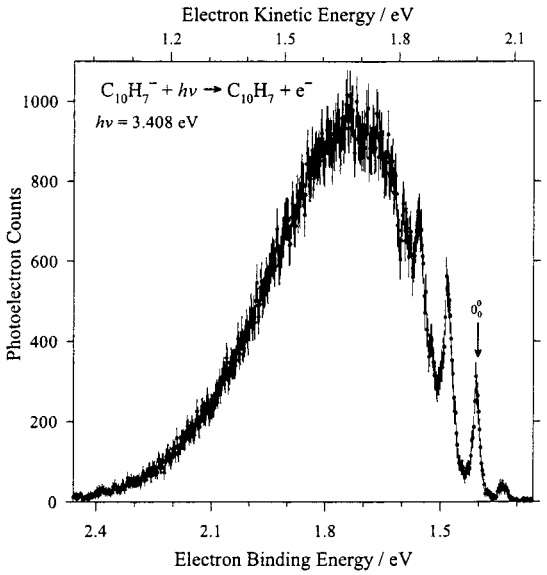

Figure 1. Experimental negative ion photoelectron spectrum of $C_{10}H_7^-$ at a laser wavelength of 364 nm ($h\nu = 3.408$ eV). The photoelectron intensities are plotted as a function of the measured electron kinetic energy (top) and the calculated electron binding energy (bottom).

not discriminate between the formation of the two isomers, 50% each of 1-$C_{10}H_7^-$ and 2-$C_{10}H_7^-$ would be produced, although the 1-$C_{10}H_7^-$ anion is slightly favored energetically (Table 1). However, the $C_{10}H_7^-$ anions can undergo further collisions with the naphthalene precursor gas, leading to exchange between the two isomers, reaction 3.

$$1\text{-}C_{10}H_7^- + C_{10}H_8 \rightleftarrows C_{10}H_8 + 2\text{-}C_{10}H_7^- \qquad (3)$$

In the limit that equilibrium is achieved at 300 K, the previous estimates of the relative gas-phase acidities at the two proton sites yield concentrations of the less stable 2-naphthyl anion isomer of 11% using $\delta\Delta_{acid}H_{298}$ from Reed and Kass[8] or 0.2% using the value from Lardin et al.[9] (see Table 1). Considering the uncertainties, as well as a possibly higher actual ion temperature of up to about 350 K on the basis of hot band intensities as discussed below, concentrations of 2-naphthyl anion from 0.01% to 53% are possible. Thus, our spectral analysis must consider the presence of both isomers in the ion beam.

The experimental photoelectron spectrum of $C_{10}H_7^-$ is presented in Figure 1. This spectrum is a composite, summed from three separate experimental sessions, but all analyses discussed below are based on the original individual spectra. The identity of the naphthyl anion (*m*/*z* 127) is assigned initially by its similarity in structure to the known[32] photoelectron spectrum of phenyl anion, $C_6H_5^-$. A broad electronic band as observed generally indicates a fairly large geometry change between the anion and neutral. A preliminary analysis, confirmed below, identifies the 0−0 vibrational origin peak at 1.4 eV electron binding energy, with several partially resolved vibrational transitions at higher electron binding energies. The origin and first vibrational transition have an observed separation of 606 ± 20 cm^{-1}, corresponding to the fundamental frequency of a mode in the neutral. A small feature at lower electron binding energy than the origin, with a separation of 560 ± 30 cm^{-1}, is either a vibrational hot band (as argued below) or else it could be due to the less stable isomer of the anion. Both of these peaks could be composed of several unresolved vibrational transitions. An attempt was made to cool the flow tube with liquid nitrogen to obtain spectra at a lower anion temperature,[33,34] but this resulted mainly in a decrease in $C_{10}H_7^-$ ion intensity, possibly due to reduction in the partial pressure of naphthalene vapor. Photoelectron spectra of the naphthyl anion band obtained while cooling the flow tube, as well as under a variety of other source conditions, showed no significant variations.

The mass resolution of the Wien filter is $m/\Delta m \approx 30$, insufficient to separate various $C_{10}H_x^-$ species in the ion beam. Under some source conditions, particularly when O^- ions are present in the flow tube, we observe weak bands in addition to $C_{10}H_7^-$ (*m*/*z* 127) that are similar to the spectrum of the *o*-benzyne anion,[35] $C_6H_4^-$, which is formed by reaction of O^- with benzene.[36] These features are therefore assigned to naphthyne anion, $C_{10}H_6^-$ (*m*/*z* 126), corresponding to H_2^+ removal from naphthalene (two isomers are possible). This spectrum has a broad transition at electron binding energies of 0.76−1.31 eV corresponding to the singlet transition in benzyne and a sharp peak at an electron binding energy of 2.50 ± 0.03 eV corresponding to the more vertical triplet transition in benzyne. The two naphthyne bands disappear simultaneously when the source conditions are optimized for $C_{10}H_7^-$ and are not analyzed further here. We also observe a weak sharp peak at a binding energy of 3.06 eV, which is assigned to a small I^- (*m*/*z* 127) impurity in the ion beam. No photodetachment at low electron binding energies is observed that could be attributed to the parent naphthalene anion, $C_{10}H_8^-$ (*m*/*z* 128). This negative result is consistent with recent studies showing that the naphthalene anion is not electronically stable in the gas phase.[37,38]

Molecular Structure Calculations

The isomeric identity of the species giving rise to the observed photoelectron spectrum cannot be determined solely on the basis of the experimental data. We use density functional theory (DFT) calculations to help distinguish the 1-$C_{10}H_7$ and 2-$C_{10}H_7$ isomers. We use DFT with the Becke3-LYP functional[39] because it has been shown to yield reliable frequencies[40,41] and it is computationally efficient for large molecules. The geometries, vibrational frequencies, and vibrational normal coordinates for the anions and neutrals of both isomers are calculated with the Becke3-LYP functional[39] and the aug-cc-pVDZ basis set[42] using Gaussian98.[43] For accurate geometries and vibrational coordinate information, the geometries were optimized with the "tight" convergence criterion and the density functional calculations used the "ultrafine" integration grid for DFT in Gaussian98.[43,44]

The calculated B3LYP/aug-cc-pVDZ geometry changes between the anion and neutral for the two isomers are depicted in Figure 2. Removal of a σ electron from the anion to form the neutral radical results in an increase in the interior CCC bond angle at the deprotonation site. For 1-$C_{10}H_7$ ← 1-$C_{10}H_7^-$ the angle increases from 112.9° to 126.6° and for 2-$C_{10}H_7$ ← 2-$C_{10}H_7^-$ the angle increases from 112.1° to 126.3°, i.e., an increase of about 14° for both isomers. This relatively large change in angle is consistent with the broad Franck−Condon profile observed in Figure 1. Complete geometry and frequency data are provided in the Supporting Information. There are several modes of each isomer that would nearly match the frequency of the observed fundamental transition.

Franck−Condon Simulation Procedure

Because the differences between the spectra of the α and β isomers are likely to be subtle, it is important that the Franck−Condon profile simulations be accurate. Many variations of methods for calculating Franck−Condon factors have been

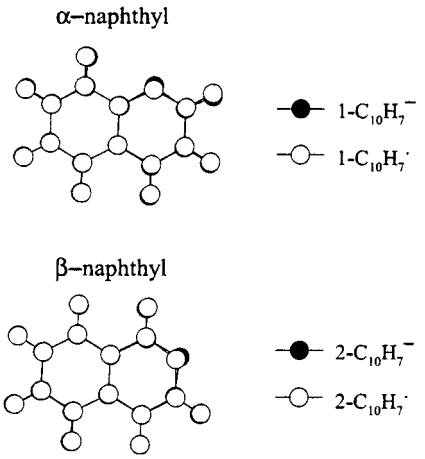

Figure 2. Geometry changes for the transitions 1-$C_{10}H_7 \leftarrow$ 1-$C_{10}H_7^-$ (α) and 2-$C_{10}H_7 \leftarrow$ 2-$C_{10}H_7^-$ (β) as calculated by density functional theory at the B3LYP/aug-cc-pVDZ level. Complete geometries are presented in the Supporting Information.

presented in the literature,[45−51] but most of these are suitable only for a small number of active modes or for 0 K spectra without hot bands. We have modified our previous procedures[26,34,52] for simulation of Franck−Condon profiles to handle large polyatomic molecules including hot bands.

The vibrational normal mode vectors in mass-weighted Cartesian coordinates for the anion, $\mathbf{Q}''$, and for the neutral, $\mathbf{Q}'$, are related by eq 4:

$$\mathbf{Q}'' = \mathbf{J}''\mathbf{Q}' + \mathbf{K}'' \tag{4}$$

where $\mathbf{J}''$ is the Duschinsky rotation matrix and $\mathbf{K}''$ is a vector of geometry displacements along each normal mode in the anion. Duschinsky rotation and the relationships between these normal mode coordinates and the internal coordinates have been described previously.[26,47,51−53] Here we determine $\mathbf{J}''$ and $\mathbf{K}''$ from the normal coordinate vectors and geometries calculated by Gaussian98, extracted from the Gaussian output files using a Fortran program (FCFGAUS) derived in part from code by Chen and co-workers.[51,54] The Eckart condition is used to ensure that $\mathbf{J}''$ does not introduce rotational motion between the two states, as described by Chen.[51]

The parallel mode approximation neglects Duschinsky rotation by setting $\mathbf{J}'' = \mathbf{I}$, the identity matrix. A major computational advantage of the parallel mode approximation is that the Franck−Condon factors for transitions involving combinations of modes are given as a product of the Franck−Condon factors for one-dimensional systems, eq 5,

$$\langle \nu_1'\nu_2'\nu_3'...\nu_n'|\nu_1''\nu_2''\nu_3''...\nu_n''\rangle^2 = \prod_{i=1}^{n}\langle \nu_i'|\nu_i''\rangle^2 \tag{5}$$

where υ_i' and υ_i'' are the number of quanta excited in mode i of the neutral and anion, respectively. In the parallel mode approximation, the normal mode displacement vector in the basis of the normal coordinates of the upper neutral state, $\mathbf{K}' = -(\mathbf{J}'')^{\mathrm{T}}\mathbf{K}''$, should be used.[52] For this purpose, FCFGAUS matches the normal coordinate vectors with the greatest overlap (largest dot product magnitudes) between the anion and neutral states. Otherwise, the vibrational modes output by Gaussian98 are ordered simply by increasing vibrational frequency, resulting in possible mismatches between the two states, especially in large polyatomic systems with many modes of similar frequencies. For both 1- and 2-naphthyl, there are several modes for which this automatic matching procedure does not give unique assignments. That is, two different modes in the anion match with a single mode in the neutral state while another mode in the upper state has a somewhat smaller dot product magnitude and is not matched. In that case, these modes are reassigned manually to maximize the overall overlap between the two states. FCFGAUS also sorts the modes so that $\mathbf{J}''$ is block diagonal, with separate blocks for the totally symmetric modes (in-plane for naphthyl) and nontotally symmetric modes (out-of-plane).

TABLE 2: Calculated Frequencies and Geometry Displacements[a]

frequency/cm^{-1}				
anion	neutral	K''/(g/mol)$^{1/2}$Å	K'/(g/mol)$^{1/2}$Å	J_{ii}
		1-$C_{10}H_7 \leftarrow$ 1-$C_{10}H_7^-$		
620.4	628.2	0.4072	−0.4302	0.9938
929.3	924.4	0.2467	−0.2400	0.9895
754.1	774.2	0.1981	−0.2203	0.9845
509.6	502.3	0.2048	−0.2264	0.9899
514.7	521.2	0.2692	−0.2098	0.9882
1116.2	1136.0	−0.1158	0.1077	0.9615
1506.9	1516.3	0.0469	−0.0490	0.9553
801.4	794.2	−0.0678	0.0664	0.9835
		2-$C_{10}H_7 \leftarrow$ 2-$C_{10}H_7^-$		
789.8	789.5	0.3352	−0.3388	0.9733
506.0	518.5	0.4207	−0.4167	0.8016
925.5	927.1	−0.2276	0.2147	0.9940
769.8	767.3	−0.0478	0.1312	0.9699
363.5	375.6	−0.1772	0.1755	0.9979
635.0	625.4	0.1139	−0.1212	0.9899
520.7	509.0	0.1396	0.1356	0.7940
1002.3	1050.1	0.1218	−0.0841	0.7473

[a] Calculated at the B3LYP/aug-cc-pVDZ level. Values for the eight most-active modes are listed; entries for all 45 modes are provided in the Supporting Information.

Table 2 presents the frequencies and displacements for the modes with the largest Franck−Condon displacements for the two isomers (the data for all modes are included in the Supporting Information). The 628 cm^{-1} frequency of the most-active mode of the 1-$C_{10}H_7$ isomer matches the 606 ± 20 cm^{-1} spacing of the observed fundamental progression, a better match than the 789 cm^{-1} and 520 cm^{-1} frequencies of the two most-active modes for 2-$C_{10}H_7$. However, because both isomers have other active modes with similar frequencies, a firm assignment without a complete simulation of the Franck−Condon profiles would be difficult.

The Franck−Condon factors are calculated by our revised Fortran program PESCAL[55] using two methods, both in the independent harmonic oscillator, normal mode approximation and including hot bands. (1) In the parallel mode approximation neglecting Duschinsky rotation, Franck−Condon factors are obtained using the recursion relation method of Hutchisson[45] with the vibrational frequencies and the $\mathbf{K}'$ displacement vector as input, as described previously.[26,52] (2) To include Duschinsky rotation, the Franck−Condon factors are calculated using the algorithm of Chen,[51] which is based upon the generating function method of Sharp and Rosenstock.[47] PESCAL is also capable of calculating Franck−Condon factors for independent Morse oscillators or other one-dimensional potentials as described previously,[25,26,52] but we limit our calculations here to harmonic oscillators because no reliable information about vibrational anharmonicities for naphthyl anions or radicals is available from either the experiment or theory.

The treatment of Duschinsky rotation requires the **A**, **C**, and **E** matrixes and **B** and **D** vectors of coefficients, as defined by Sharp and Rosenstock,[47] which are calculated by PESCAL from

J″, **K″**, and the vibrational frequencies. For cold bands, transitions from the ground vibrational state of the anion, the Chen algorithm is used directly with code adapted from Chen and co-workers.[54] For hot bands, transitions from vibrationally excited anions, we have corrected the Chen algorithm on the basis of comparison with the direct power series expansion method of Sharp and Rosenstock. In particular, whereas the **A** and **C** matrixes are symmetric and only the coefficients in the upper or lower triangle are needed, the **E** matrix is nonsymmetric, leading to various terms for hot combination bands (i.e., $\langle ...v_i'v_j'...|...v_i''v_j''...\rangle$ transitions) including the matrix elements E_{ij} and E_{ji} that were not properly included by Chen.[51,54] The Franck−Condon factor expressions generated by the corrected Chen algorithm have been verified using a symbolic mathematics program (MapleV, Waterloo Maple, Inc.) to carry out the Sharp and Rosenstock power series expansion explicitly. This procedure avoids errors that easily arise—both the table of factor expressions in the original Sharp and Rosenstock paper[47] and the corrected and extended table by Botter et al.[56] contain typographic or algebraic errors. Explicit expressions for the Franck−Condon factors for selected transitions are included in the Supporting Information for reference.

For polyatomic molecules, the number of possible vibrational transitions and therefore the computational effort grows factorially with the number of modes and neutral or anion quanta excited. For naphthyl with 17 atoms and 45 vibrational modes, calculating or even explicitly enumerating all possible transitions is computationally prohibitive. The total number of vibrational states (all combinations of modes) for the neutral 1-naphthyl radical up to 1 eV above the origin is 1.1×10^{10} as calculated using the Beyer−Swinehart algorithm.[57] With the inclusion of vibrationally excited anions, the number of possible transitions expands enormously. Fortunately, the vast majority of these transitions have small Franck−Condon factors or anion state populations and can be neglected. We have implemented[55] an "intelligent" scheme that attempts to calculate only the important transitions: (1) We start by stepping through the levels of the upper state by incrementing the first mode up to a predetermined maximum number of quanta, then carrying over to the next mode. The maximum level for each mode is set by energy limits and by single-mode Franck−Condon factors. (2) If any transition is above the energy limit for the simulation, all higher transitions involving that mode are skipped and the next mode is incremented. (3) If any transition intensity is below a cutoff value, a test is made whether higher levels of that mode can be skipped. This test is based on the normal profiles of Franck−Condon bands for harmonic oscillators and relies on the single-mode Franck−Condon factors for the currently incrementing mode. Specifically, higher levels are skipped if both $\langle v' + 1|v''\rangle^2$ and $\langle v' + 2|v''\rangle^2$ are less than $\langle v'|v''\rangle^2$ and if $v' \geq v''$ for that mode. (4) After incrementing through all modes of the upper state, the lower state levels are incremented mode by mode in an outer loop. (5) We take advantage of the sparsity of the number of modes excited in many transitions by reducing the calculation of each transition to only those modes with excitations in either the anion or the neutral state. (6) Individual transition intensities are binned according to the transition energy as they are calculated for subsequent convolution over the instrumental resolution function.

Even with these optimizations, the calculation including Duschinsky rotation is slow when many modes or high quantum levels are excited. We can further reduce the calculation by taking advantage of the block-diagonal nature of **J″**, which means that the totally symmetric vibrational modes do not have Duschinsky mixing with nontotally symmetric modes. Therefore, the Franck−Condon factor is the product of two smaller calculations, eq 6,

$$\langle \nu_1'\nu_2'\nu_3'...\nu_n'|\nu_1''\nu_2''\nu_3''...\nu_n''\rangle^2 = \langle \nu_1'\nu_2'\nu_3'...\nu_{n(\alpha')}|\nu_1''\nu_2''\nu_3''...\nu_{n(\alpha')}''\rangle^2 \times \langle \nu_1'\nu_2'\nu_3'...\ \nu_{n(\alpha'')}|\nu_1''\nu_2''\nu_3''...\nu_{n(\alpha'')}''\rangle^2 \quad (6)$$

where $n(a')$ is the number of totally symmetric modes and $n(a'')$ is the number of nontotally symmetric modes. Equation 6 can represent a huge time saving because the computational effort depends factorially on the number of modes. Also, the Franck−Condon factors for the nontotally symmetric transitions need be calculated only once, and then can be applied multiplicatively to the previously calculated distribution of transitions and intensities (stick spectrum) for the totally symmetric modes, with the appropriate energy offsets.

A further increase in speed can be obtained by a compromise between the parallel mode approximation and the full Duschinsky treatment. We use the multiplicative approximation given by eq 7,

$$\langle \nu_1'\nu_2'\nu_3'...\nu_n'|\nu_1''\nu_2''\nu_3''...\nu_n''\rangle^2 = \langle \nu_1'\nu_2'\nu_3'...\nu_m'0_{m+1}...0_n|\nu_1''\nu_2''\nu_3''...\nu_m''0_{m+1}...0_n\rangle^2 \times \prod_{i=m+1}^{n} \langle 0_1...0_{i-1}\nu_i'0_{i+1}...0_n|0_1...0_{i-1}\nu_i''0_{i+1}...0_n\rangle^2 \quad (7)$$

where 0_i means zero quanta are excited in mode i. In eq 7, m modes with significant Duschinsky mixing are treated exactly but the remaining modes are calculated as a product of single-mode transitions (precalculated and stored). The diagonal matrix elements of the **J″** Duschinsky matrix, J_{ii}'', are used to gauge whether individual modes need to be treated exactly. For the naphthyl spectrum, we find that the criterion $|J_{ii}''| > 0.97$ for using the multiplicative approximation for mode i yields results that are in near-exact agreement with the full Duschinsky treatment.

PESCAL further allows frequencies, geometry displacements, hot band temperatures, peak widths, the energy of the origin, and overall band intensities to be optimized by nonlinear least-squares fits to experimental spectra. In the present work, only the electron affinity (energy of the origin), overall band intensity (scaling factor), peak widths, and anion temperatures are optimized to fit the experimental spectra.

Performance of the Franck−Condon Simulations

Initially considering cold bands only (0 K anions), for 1-naphthyl a converged Franck−Condon simulation (band profile within 1%) requires including the 17 most-active modes with a cutoff threshold of 0.001% relative to the origin. At this level, 5.5×10^4 transition intensities are above the cutoff out of the 10^{10} possible transitions up to 1 eV. On a 733 MHz Pentium III computer, our optimized simulation requires 0.2 s for the parallel mode approximation with the Hutchisson method, 67 s with Duschinsky rotation using the modified Chen algorithm for each of the 17 modes, or 0.9 s using eq 7 with $|J_{ii}| > 0.97$ as the criterion for using the multiplicative approximation. For comparison, the same calculation requires 4.2 h with Duschinsky rotation but using simple nested loops over each mode, i.e., without our "intelligent" transition selection algorithm and other coding optimizations. Figure 3a compares the parallel mode approximation with the full Duschinsky

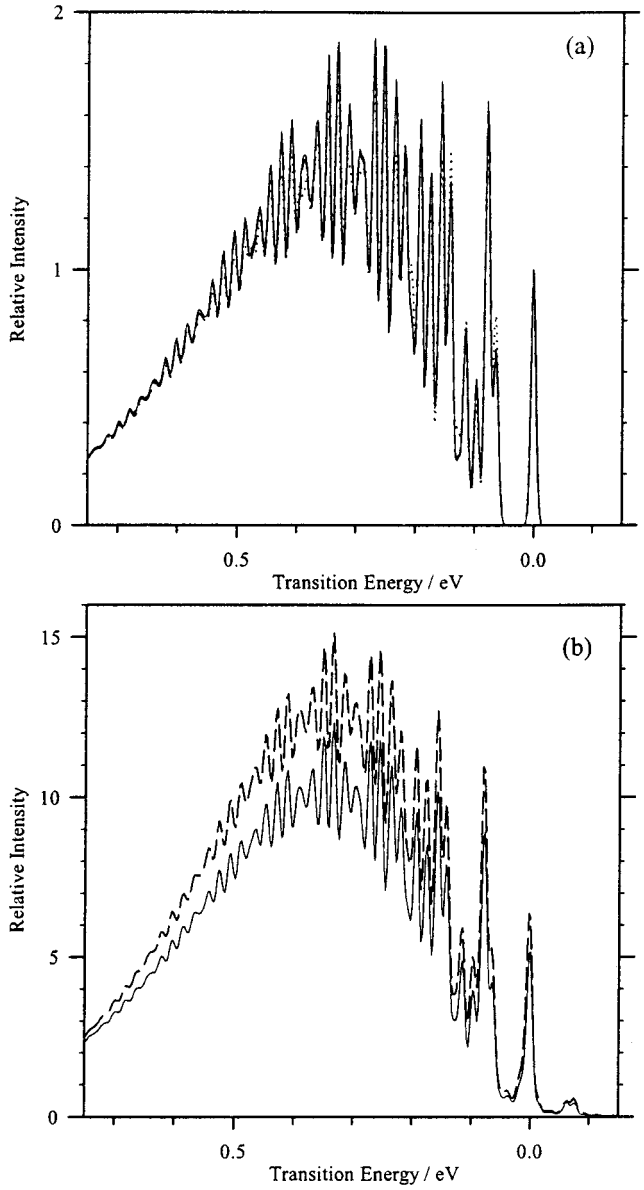

Figure 3. (a) Comparison of the simulated Franck−Condon profiles for the 1-$C_{10}H_7$ ← 1-$C_{10}H_7^-$ band at 0 K using the full Duschinsky rotation treatment (solid line), the parallel-mode approximation with **K′** displacements (dashed line, but indistinguishable from the full Duschinsky treatment), and the parallel-mode approximation with **K″** displacements (dotted line). (b) Comparison of the simulations at 300 K using the full Duschinsky treatment (solid line) and the parallel-mode approximation with **K′** displacements (dashed line). The simulations use a relative origin intensity of 1.0 and are convoluted with a Gaussian with 10 meV fwhm. See text for detailed descriptions.

treatment. For this system there is no significant difference between the Duschinsky treatment and the parallel-mode approximation, despite the 14° bond angle change between the anion and neutral. Indeed, Duschinsky rotation will be important only when there is *both* a large geometry change between the two states *and* a significant change in the normal coordinate vector directions for *active* modes. Examination of the diagonal matrix elements of **J″** (Table 2) shows that the five modes with the largest Franck−Condon activity for 1-$C_{10}H_7$ have $|J_{ii}| > 0.98$, where $|J_{ii}| = 1$ would indicate completely parallel normal coordinate vectors in the two states. Although 2-$C_{10}H_7$ exhibits greater Duschinsky mixing (Table 2), the top five modes are not strongly mixed among themselves (but rather with other weaker modes) and the simulation still shows no significant difference with and without the Duschinsky treatment. The relative rigidity of the two-ring system in naphthyl may be responsible for the lack of importance of Duschinsky rotation, by limiting the geometry change to just the puckering of the ring at the deprotonation state. In general, for the case of a large geometry change one would also expect anharmonicity effects to be important, perhaps more important than Duschinsky rotation.[52] Because the partially resolved bands in the present work are at low energy, we do not expect anharmonicity to be important here. Finally, if the geometry displacements in the anion basis (**K″**) are improperly used instead of the neutral basis (**K′**) for the parallel mode approximation, then there are noticeable deviations from the treatment with Duschinsky rotation, as also shown in Figure 3a.

Because the 1-naphthyl anion has several low-frequency modes (164, 170, 380, 401, 498, ... cm^{-1}; see the Supporting Information), at 300 K the ground vibrational state of 1-$C_{10}H_7^-$ has a fractional Boltzmann population of only 11%. The majority of the band intensity arises from hot ($v_i'' > 0$) or sequence ($v_i'' > 0$ and $v_i' = v_i''$) bands, and therefore convergence of the simulated Franck−Condon profile is more difficult when hot bands are included. With all 45 modes included, using a cutoff of 0.00001% relative to the origin, and with the parallel mode approximation, 1.3×10^8 transitions have intensities above the cutoff and the computer time required is 90 min. The same simulation including Duschinsky rotation using eq 7 requires 30 h. In both cases most of the computational time (98% and 99.8%, respectively) is spent on the low-frequency nontotally symmetric (out-of-plane) modes. The two simulations are compared in Figure 3b. Although the profiles are very similar, the simulation with Duschinsky rotation has intensities about 25% smaller than the parallel mode approximation. Duschinsky effects become significant when hot bands are included in the simulation primarily because the low-frequency out-of-plane modes, which have large thermal populations and contribute to sequence bands, have strong Duschinsky mixing. However, because the sequence bands are not resolved here, these modes mainly result in the broadening of the vibrational peaks and their inclusion is not critical to the interpretation of the spectra.

To test the sensitivity of the simulations to the level of molecular structure theory, we repeated them using HF/6-31+G(d) and HF/6-311+G(df,p) calculations instead of B3LYP/aug-cc-pVDZ. These simulations (compared in Figure 3S in the Supplementary Information) show the same overall band profile and similar relative intensities of the low-energy peaks in the resolved region of the experimental spectrum. There are minor differences at higher energies, where the experimental spectrum is unresolved. We also attempted a calculation at the MP2/6-31+G(d) level, but it gave a spurious high negative frequency for an out-of-plane twist mode of the neutral radical despite a reasonable geometry from an unconstrained optimization. We have not investigated the reason for the spurious frequency, but instabilities in HF and MP2 frequencies are not unprecedented.[58]

Comparison of Simulated and Experimental Spectra

Figure 4 compares the simulated Franck−Condon profiles for 1-$C_{10}H_7^-$ and 2-$C_{10}H_7^-$ with the experimental spectrum. The simulations shown are calculated with the Duschinsky treatment for all 45 modes using the multiplicative approximation (eq 7) for modes with $|J_{ii}| > 0.97$, an anion temperature of 300 K, and a Gaussian resolution function with a 17 meV full-width at half-maximum (fwhm). Sequence bands account for an additional 5−7 meV apparent width of the transitions at 300

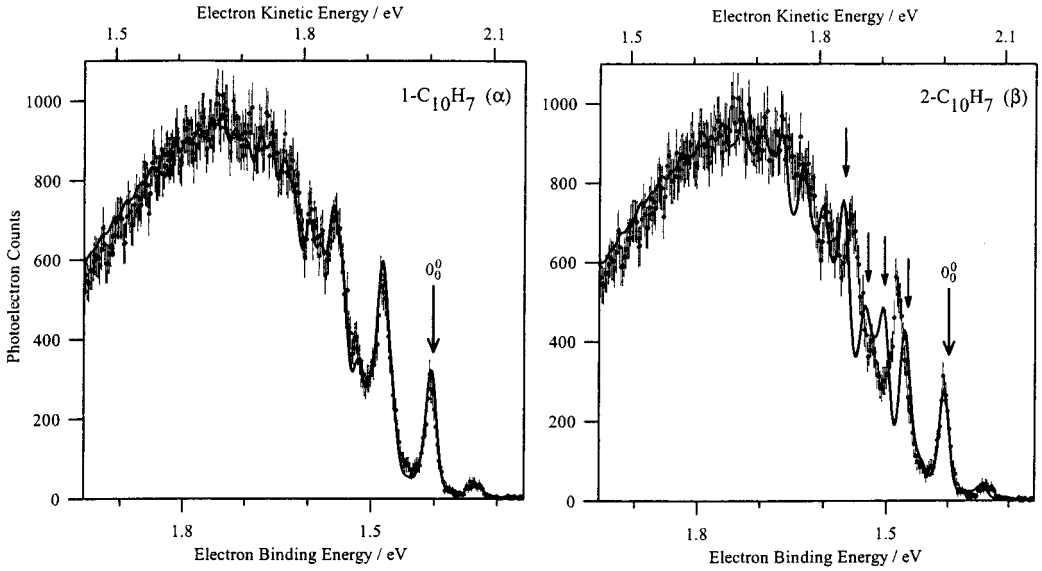

Figure 4. Comparison of the experimental spectrum with the simulated Franck−Condon profile for 1-$C_{10}H_7$ ← 1-$C_{10}H_7^-$ (left panel) and 2-$C_{10}H_7$ ← 2-$C_{10}H_7^-$ (right panel). Arrows mark the 0_0^0 origins for each spectrum and significant mis-matches for the 2-$C_{10}H_7$ simulation.

K. Higher temperatures increase the peak widths because of the sequence bands, allowing instrumental resolution functions closer to the values of 10−15 meV fwhm observed for O^- or NH_2^- under the experimental conditions, but make no difference in the overall quality of the fits. Anion temperatures higher than 350 K can be excluded by the small intensities of the observed hot bands. Because of the small rotational constants for these heavy molecules, rotational broadening is negligible. No spin−orbit state splittings are expected for the $^2A' \leftarrow {}^1A'$ electronic transition. The isomerization barriers between the α and β anions and radicals are expected to be high, but presence of a mixture of the two naphthyl anion isomers is a possible additional source of peak broadening.

The two simulated profiles are similar overall, as expected from the similar geometry displacements for the α and β isomers as shown in Figure 2, but there are significant differences for the first few transitions above the origin. For 1-$C_{10}H_7^-$ the simulation is in excellent agreement with the experiment, but for 2-$C_{10}H_7^-$ the simulation shows several transitions (marked by arrows in Figure 4) that do not match the experimental peak positions and intensities. On the basis of these simulations, we assign the observed spectrum as being primarily due to 1-$C_{10}H_7^-$ and we confirm the assignment of the origin transition at 2.005 ± 0.015 eV electron kinetic energy, leading to EA_0(1-$C_{10}H_7$) = 1.403 ± 0.015 eV.

The calculated hot band transitions at 300 K for the 1-naphthyl isomer account for all or most of the observed hot band intensity near 1.34 eV electron binding energy. According to the relative gas-phase acidities from kinetic experiments,[8,9] some 2-$C_{10}H_7^-$ could be present in the ion beam (vide supra). In the equilibrium limit, the populations of the two anions in the flow tube source depend on $\delta\Delta_{acid}H$. The spacing of the origin peaks in the photoelectron spectrum for the two anions depends on δEA. According to eq 1, these are related by $\delta D \approx \delta\Delta_{acid}H + \delta$EA. Figure 5 compares simulations for both states together with relative energies of δEA = 0, 0.02, 0.04, and 0.06 eV, using the approximation δEA ≈ $-\delta\Delta_{acid}H$ (i.e., that $\delta D \approx$ 0 or that the $C_{10}H_7$−H bond dissociation energies are the same for the two isomers) and relative populations based on equilibrium populations at 300 K. Specifically, we approximate that $\delta\Delta_{acid}H = \delta\Delta_{acid}G$ so that the fractional population of the 2-$C_{10}H_7^-$ isomer is given by $e^{-\delta EA/RT}/(1 + e^{-\delta EA/RT})$. We make the reasonable further assumption that the two isomers have the same overall photodetachment cross section magnitudes. Comparing these simulations with the experimental spectrum in Figure 5, it is apparent that values of δEA of 0.04 eV and below show significant deviations from experiment, whereas the simulation for δEA = 0.06 eV agrees reasonably with experiment. For δEA = 0.06 eV, the 2-$C_{10}H_7^-$ isomer has a fractional population of only 9% and its origin is partially hidden by the hot band transition for 1−$C_{10}H_7^-$. A larger δEA, for which 2-$C_{10}H_7^-$ would not be present in observable quantities, is also consistent with the data. We assign a lower limit of δEA ≥ 0.05 eV on the basis of these simulations. From our data alone we cannot rigorously eliminate the possibility that $\delta D \neq 0$, i.e., the possibility that the apparent absence of the 2-$C_{10}H_7^-$ anion is due to a low gas-phase acidity equilibrium concentration that is not also reflected in a δEA difference. However, both the kinetic experiments[8,9] and theory[2] support $\delta D \approx 0$.

Thermochemistry

The present experiments provide the electron affinity for the α-naphthyl radical, EA_0(1-$C_{10}H_7$) = 1.403 ± 0.015 eV, and support previous kinetic studies[8,9] that the α-naphthyl anion is thermochemically more stable than the β-naphthyl anion. The absolute electron affinity agrees with those obtained by the Cooks kinetic method (Table 1),[8,9] with at least touching error bars. Our limit of δEA ≥ 0.05 eV is in good accord with the relative electron affinities of the two isomers obtained by the kinetic method (Table 1). Because we now have a more accurate and precise absolute electron affinity for 1-naphthyl radical, it is useful to obtain EA(2-$C_{10}H_7$) by combining our value for EA(1-$C_{10}H_7$) with the relative electron affinity, δEA, from the kinetic experiments as shown in Table 1. Combining the average value for δEA from the kinetics experiments with our limit of δEA ≳ 0.05 eV from this work and anchoring to our absolute electron affinity for 1-$C_{10}H_7$, we obtain an estimate of EA(2-$C_{10}H_7$) = $1.34^{+0.03}_{-0.07}$ eV.

Equation 1 provides a means to derive the CH bond dissociation energy from the electron affinity of the radical and the gas-phase acidity of the parent molecule. To obtain the best possible values for the bond dissociation energies of naphthalene at the α and β positions, it is necessary to reevaluate the

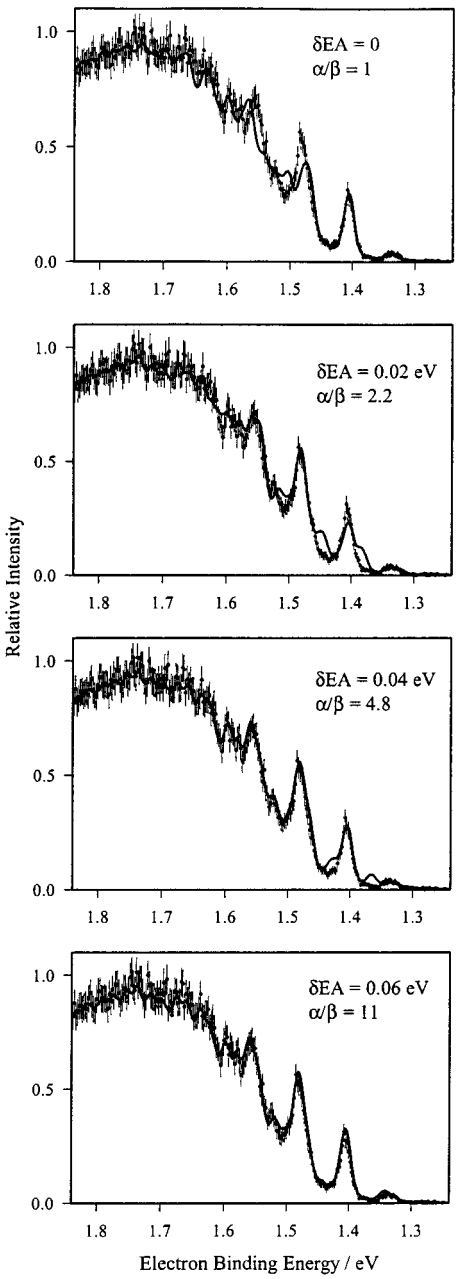

Figure 5. Franck−Condon simulations for combined 1-$C_{10}H_7$ ← 1-$C_{10}H_7^-$ and 2−$C_{10}H_7$ ← 2-$C_{10}H_7^-$ spectra assuming various values of $\delta EA \approx \delta\Delta_{acid}H$, as described in the text.

literature values for the absolute gas-phase acidities. The gas-phase acidity of naphthalene from pulsed high-pressure mass spectrometry equilibrium measurements by Meot-Ner et al.[13] is now confirmed to refer to formation of the α anion isomer, $C_{10}H_8 \rightarrow$ 1-$C_{10}H_7^- + H^+$. Meot-Ner et al.[13,59] measured the equilibrium constants for proton transfer of naphthyl anions with benzene, 1,4-diazine, and water in the temperature range 500−625 K. These experiments represent the only equilibrium measurement of the gas-phase acidity of naphthalene, but they bear reexamination in light of recently revised values of the gas-phase acidities of benzene and water,[7,60] the possible presence of the 2-naphthyl anion isomer,[8,9] and temperature corrections. Table 3 lists current literature values for water, benzene, and ammonia (relative to which the acidity of benzene was measured[7]). Unfortunately, the gas-phase acidity reported by Meot-Ner et al.[13] cannot be simply adjusted using the more up-to-date values for water and benzene, because it was obtained by averaging relative acidities in a ladder of individual measurements and was apparently anchored to $\Delta_{acid}H$ values for calibration acids at 298 K instead of 600 K. Instead, we use the original equilibrium measurements of ln K_{600} for individual reactions as obtained from figures published by Meot-Ner et al.[13,59] These are converted to $\delta\Delta_{acid}G_{600} = -RT \ln K_{600}$ to obtain the ladder of values shown in Figure 6. We use a least-squares optimization as described elsewhere[61] to obtain the best value for $\Delta_{acid}G_{600}(C_{10}H_8)$ with H_2O and C_6H_6 as anchor acids. Temperature corrections for $\Delta G(T)$, $\Delta S(T)$, and $\Delta H(T)$ are calculated as required using values in Gurvich et al.[62,63] if available or using standard statistical mechanics formulas[7,64] in the harmonic-oscillator rigid-rotor approximation with the theoretical molecular constants calculated in this work or the literature.[7] We obtain $\Delta_{acid}G_{600}(C_{10}H_8) = 1565 \pm 13$ kJ/mol from the least-squares optimization, which yields $\Delta_{acid}H_{298}(C_{10}H_8) = 1642 \pm 13$ kJ/mol after enthalpy and entropy temperature corrections. This can be compared with Meot-Ner's originally reported value of $\Delta_{acid}H_{298}(C_{10}H_8) = 1649 \pm 5$ kJ/mol. Our larger error bar (an estimate of ±2 combined standard uncertainties[65]) reflects internal inconsistencies in the overlapping $\delta\Delta G$ values in the acidity ladder in Figure 6, a 10 kJ/mol mismatch with the relative acidities of H_2O and C_6H_6 compared with literature values, and the possible presence of 2-$C_{10}H_7^-$ anions in equilibrium with 1-$C_{10}H_7^-$. (The $\delta\Delta_{acid}G$ values in parentheses in Figure 6 are corrected for the possible presence of 2-$C_{10}H_7^-$ in the extreme case of a unity equilibrium constant for reaction 3, $\delta\Delta_{acid}G = 0$. This would lower $\Delta_{acid}G_{600}$(1-$C_{10}H_7$−H) by several kJ/mol, but does not improve the internal consistency of the ladder. Furthermore, the effect is <1 kJ/mol if one uses the $\delta\Delta_{acid}G$ values measured by the kinetics experiments.)

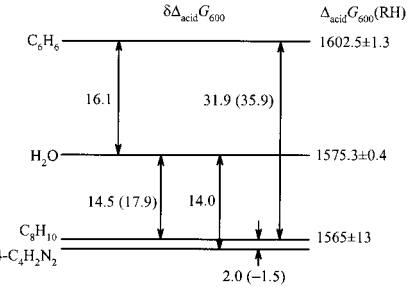

Figure 6. Gas-phase acidity ladder of relative $\delta\Delta_{acid}G_{600}$ (kJ/mol) measurements taken from Meot-Ner et al.,[13,59] with absolute anchor values for water and benzene from Table 3. See text for details.

TABLE 3: Literature and Derived Thermochemical Values[a]

R	$EA_0(R)$/eV	$D_0(RH)$	$\Delta_{acid}H_0(RH)$	$\Delta_{acid}H_{298}(RH)$	$\Delta_{acid}G_{298}(RH)$	$\Delta_{acid}G_{600}(RH)$
HO	1.8277 ± 0.0004[b]	491.91 ± 0.38[c]	1627.7 ± 0.3[c]	1632.6 ± 0.3[c]	1605.0 ± 0.3[c]	1575.3 ± 0.4
NH_2	0.771 ± 0.005[d]	444.0 ± 0.2[e]	1681.7 ± 0.5	1687.7 ± 0.6	1657.0 ± 1.2	
C_6H_5	1.097 ± 0.006[f]	466.4 ± 1.4	1672.6 ± 1.3	1678.9 ± 1.3	1642.0 ± 1.2[g]	1602.5 ± 1.3

[a] In kJ/mol except as noted. Values without footnotes are obtained using the negative ion cycle, eq 1, and $IE_0(H)$[67] = 1312.0494 ± 0.0001 kJ/mol or by conversion from 298 K gas-phase acidities. Enthalpy and entropy thermal corrections are taken from Gurvich et al.[62,63] where available or are calculated using standard statistical mechanical formulas in the harmonic-oscillator rigid-rotor approximation. [b] Ref 68. [c] Ref 60, 69. [d] Ref 28. [e] Ref 70. [f] Reference 32. [g] Calculated relative to ammonia using $\Delta_{acid}G_{300}(C_6H_6) - \Delta_{acid}G_{300}(NH_3) = -14.98 \pm 0.25$ kJ/mol from ref 7.

Equilibrium measurements of gas-phase acidities are usually preferred over those obtained by the DePuy silane cleavage kinetics method, and both Reed and Kass[8] and Lardin et al.[9] referenced their relative values to the absolute acidity of Meot-Ner et al.[13] to calculate the bond dissociation energy. However, the reevaluated equilibrium value is not more precise than the acidities from the kinetics measurements for the reasons given above. On the other hand, the two kinetics experiments could be subject to similar systematic errors related to the nature of the dissociation transition state. For example, the silane cleavage method was shown to fail in its application to cubane,[66] although naphthalene does not have the same issues with possible rehybridization implicated for cubane. Pending a definitive independent measurement of the acidity, we average the measurements to obtain a recommended value of $\Delta_{acid}H_{298}$(1-$C_{10}H_7$−H) = 1649 ± 14 kJ/mol. The main effect of this reevaluation is to recommend a larger, more realistic uncertainty.

Finally, we use eq 1 to obtain the CH bond dissociation enthalpy of naphthalene, D_{298}(1-$C_{10}H_7$−H) = 472 ± 14 kJ/mol, and using the average value for δD_{298} from the kinetics studies (Table 1) we obtain D_{298}(2-$C_{10}H_7$−H) = 476 ± 20 kJ/mol. As concluded in the original kinetics studies of the relative values, the two sites have the same dissociation energies within the experimental uncertainties.[8,9]

Summary

The photoelectron spectrum of $C_{10}H_7^-$ has been measured and assigned to the 1-$C_{10}H_7$ ← 1-$C_{10}H_7^-$ transition by comparison with Franck−Condon simulations for the two possible isomers. Optimized algorithms for simulating the Franck−Condon profiles of large polyatomic molecules using calculated vibrational parameters have been presented. The simulation allows us to distinguish the 1-$C_{10}H_7$ and 2-$C_{10}H_7$ isomers, which would not be possible from the experiments alone.

We obtain an electron affinity for the 1-$C_{10}H_7$ radical, EA_0(1-$C_{10}H_7$) = 1.403 ± 0.015 eV, in general agreement with but more precise than recent kinetic method studies. A reevaluation of literature experiments for the gas-phase acidity of naphthalene[8,9,13] leads to recommended values of $\Delta_{acid}H_{298}$(1-$C_{10}H_7$−H) = 1649 ± 14 kJ/mol and D_{298}(1-$C_{10}H_7$−H) = 472 ± 14 kJ/mol. This does not significantly change the nominal bond dissociation energy from previous reports,[8,9] but places a larger and more realistic uncertainty on the value. A more precise experimental determination of the bond dissociation energy using the negative ion thermochemical cycle will require a definitive independent measurement of the gas-phase acidity of naphthalene.

Acknowledgment. This work was supported by the U.S. Department of Energy, Office of Science, Office of Basic Energy Sciences, Division of Chemical Sciences, Geosciences, and Biosciences (University of Nevada), and by the National Science Foundation (JILA).

Supporting Information Available: DFT geometries and frequencies of 1-naphthyl and 2-naphthyl radicals and anions and naphthalene. Sharp and Rosenstock expressions for Franck−Condon factors. This material is available free of charge via the Internet at http://pubs.acs.org.

References and Notes

(1) Wang, H.; Frenklach, M. *J. Phys. Chem.* **1994**, *98*, 11465.
(2) Barckholtz, C.; Barckholtz, T. A.; Hadad, C. M. *J. Am. Chem. Soc.* **1999**, *121*, 491.
(3) Cook, D. J.; Saykally, R. J. *Astrophys. J.* **1998**, *493*, 793.
(4) Hecht, S. S.; Carmella, S. G.; Murphy, S. E.; Foiles, P. G.; Chung, F. L. *J. Cell. Biochem. Suppl.* **1993**, *17F*, 27.
(5) Pope, C. J.; Marr, J. A.; Howard, J. B. *J. Phys. Chem.* **1993**, *97*, 11001.
(6) Richter, H.; Mazyar, O. A.; Sumathi, R.; Green, W. H.; Howard, J. B.; Bozzelli, J. W. *J. Phys. Chem. A* **2001**, *105*, 1561.
(7) Davico, G. E.; Bierbaum, V. M.; DePuy, C. H.; Ellison, G. B.; Squires, R. R. *J. Am. Chem. Soc.* **1995**, *117*, 2590.
(8) Reed, D. R.; Kass, S. R. *J. Mass Spectrom.* **2000**, *35*, 534.
(9) Lardin, H. A.; Squires, R. R.; Wenthold, P. G. *J. Mass Spectrom.* **2001**, *36*, 607.
(10) Cioslowski, J.; Liu, G.; Martinov, M.; Piskorz, P.; Moncrieff, D. *J. Am. Chem. Soc.* **1996**, *118*, 5261.
(11) Ervin, K. M. *Chem. Rev.* **2001**, *101*, 391.
(12) Berkowitz, J.; Ellison, G. B.; Gutman, D. *J. Phys. Chem.* **1994**, *98*, 2744.
(13) Meot-Ner (Mautner), M.; Liebman, J. F.; Kafafi, S. A. *J. Am. Chem. Soc.* **1988**, *110*, 5937.
(14) DePuy, C. H.; Bierbaum, V. M.; Damrauer, R. *J. Am. Chem. Soc.* **1984**, *106*, 4051.
(15) DePuy, C. H.; Gronert, S.; Barlow, S. E.; Bierbaum, V. M.; Damrauer, R. *J. Am. Chem. Soc.* **1989**, *111*, 1968.
(16) Wenthold, P. G.; Hu, J.; Squires, R. R. *J. Am. Chem. Soc.* **1996**, *118*, 11865.
(17) McLuckey, S. A.; Cameron, D.; Cooks, R. G. *J. Am. Chem. Soc.* **1981**, *103*, 1313.
(18) Cooks, R. G.; Koskinen, J. T.; Thomas, P. D. *J. Mass Spectrom.* **1999**, *34*, 85.
(19) Armentrout, P. B. *J. Am. Soc. Mass Spectrom.* **2000**, *11*, 371.
(20) Wenthold, P. G. *J. Am. Soc. Mass Spectrom.* **2000**, *11*, 601.
(21) Ervin, K. M. *Int. J. Mass Spectrom.* **2000**, *195/196*, 271.
(22) Drahos, L.; Vékey, K. *J. Mass Spectrom.* **1999**, *34*, 79.
(23) Armentrout, P. B. *J. Mass Spectrom.* **1999**, *34*, 74.
(24) Leopold, D. G.; Murray, K. K.; Stevens Miller, A. E.; Lineberger, W. C. *J. Chem. Phys.* **1985**, *83*, 4849.
(25) Ervin, K. M.; Ho, J.; Lineberger, W. C. *J. Chem. Phys.* **1989**, *91*, 5974.
(26) Ervin, K. M.; Lineberger, W. C. In *Advances in Gas-Phase Ion Chemistry*; Adams, N. G., Babcock, L. M., Eds.; JAI: Greenwich, CT, 1992; Vol. 1, p 121.
(27) Neumark, D. M.; Lykke, K. R.; Andersen, T.; Lineberger, W. C. *Phys. Rev. A* **1985**, *32*, 1890.
(28) Wickham-Jones, C. T.; Ervin, K. M.; Ellison, G. B.; Lineberger, W. C. *J. Chem. Phys.* **1989**, *91*, 2762.
(29) Blondel, C. *Phys. Scr.* **1995**, *T58*, 31.
(30) Mohr, P. J.; Taylor, B. N. *J. Phys. Chem. Ref. Data* **1999**, *28*, 1713. (http://physics.nist.gov/cuu/Constants/).
(31) Bartmess, J. E. In *NIST Chemistry WebBook, NIST Standard Reference Database Number 69*; Mallard, W. G., Linstrom, P. J., Eds.; National Institute of Standards and Technology: Gaithersburg, MD, Feb. 2000. (http://webbook.nist.gov).
(32) Gunion, R. F.; Gilles, M. K.; Polak, M. L.; Lineberger, W. C. *Int. J. Mass Spectrom. Ion Processes* **1992**, *117*, 601.
(33) Robinson, M. S.; Polak, M. L.; Bierbaum, V. M.; DePuy, C. H.; Lineberger, W. C. *J. Am. Chem. Soc.* **1995**, *117*, 6766.
(34) Wenthold, P. G.; Polak, M. L.; Lineberger, W. C. *J. Phys. Chem.* **1996**, *100*, 6920.
(35) Wenthold, P. G.; Squires, R. R.; Lineberger, W. C. *J. Am. Chem. Soc.* **1998**, *120*, 5279.
(36) Wenthold, P. G.; Hu, J.; Squires, R. R. *J. Mass Spectrom.* **1998**, *33*, 796.
(37) Lyapustina, S.; Xu, S.; Nilles, J. M.; Bowen, K. H., Jr. *J. Chem. Phys.* **2000**, *112*, 6643.
(38) Schiedt, J.; Knott, W. J.; Le Barbu, K.; Schlag, E. W.; Weinkauf, R. *J. Chem. Phys.* **2000**, *113*, 9470.
(39) Becke, A. D. *J. Chem. Phys.* **1993**, *98*, 5648.
(40) Wong, M. W. *Chem. Phys. Lett.* **1996**, *256*, 391.
(41) Halls, M. D.; Velkovski, J.; Schlegel, H. B. *Theor. Chem. Acc.* **2001**, *105*, 413.
(42) Woon, D. E.; Dunning, T. H., Jr. *J. Chem. Phys.* **1993**, *98*, 1358.
(43) Frisch, M. J.; Trucks, G. W.; Schlegel, H. B.; Scuseria, G. E.; Robb, M. A.; Cheeseman, J. R.; Zakrzewski, V. G.; Montgomery, J. A., Jr.; Stratmann, R. E.; Burant, J. C.; Dapprich, S.; Millam, J. M.; Daniels, A. D.; Kudin, K. N.; Strain, M. C.; Farkas, O.; Tomasi, J.; Barone, V.; Cossi, M.; Cammi, R.; Mennucci, B.; Pomelli, C.; Adamo, C.; Clifford, S.; Ochterski, J.; Petersson, G. A.; Ayala, P. Y.; Cui, Q.; Morokuma, K.; Malick, D. K.; Rabuck, A. D.; Raghavachari, K.; Foresman, J. B.; Cioslowski, J.; Ortiz, J. V.; Stefanov, B. B.; Liu, G.; Liashenko, A.; Piskorz, P.; Komaromi, I.; Gomperts, R.; Martin, R. L.; Fox, D. J.; Keith, T.; Al-Laham, M. A.; Peng, C. Y.; Nanayakkara, A.; Gonzalez, C.; Challacombe, M.; Gill, P. M. W.; Johnson, B.; Chen, W.; Wong, M. W.; Andres, J. L.; Gonzalez, C.; Head-Gordon, M.; Replogle, E. S.; Pople, J. A. *Gaussian98*, Revision A.6; Gaussian, Inc.: Pittsburgh, PA, 1998.

(44) Ochterski, J. W. *Vibrational Analysis in Gaussian*; http://www-.Gaussian.com/vib.htm Gaussian, Inc., 1999.
(45) Hutchisson, E. *Phys. Rev.* **1930**, *36*, 410.
(46) Hutchisson, E. *Phys. Rev.* **1931**, *37*, 45.
(47) Sharp, T. E.; Rosenstock, H. M. *J. Chem. Phys.* **1964**, *41*, 3453.
(48) Chau, F.-t.; Dyke, J. M.; Lee, E. P.-f.; Wang, D.-c. *J. Electron Spectrosc. Related Phenom.* **1998**, *97*, 33. (See also refs 1−25 therein.)
(49) Mok, D. K. W.; Lee, E. P. F.; Chau, F.-T.; Wang, D.; Dyke, J. M. *J. Chem. Phys.* **2000**, *113*, 5791. (See also refs 21−30 therein.)
(50) Mebel, A. M.; Hayashi, M.; Liang, K. K.; Lin, S. H. *J. Phys. Chem. A* **1999**, *103*, 10674. (See also refs 38−75 therein.)
(51) Chen, P. In *Unimolecular and Bimolecular Reactions Dynamics*; Ng, C.-Y., Baer, T., Powis, I., Eds.; John Wiley & Sons: Chichester, 1994; p 371.
(52) Ervin, K. M.; Ho, J.; Lineberger, W. C. *J. Phys. Chem.* **1988**, *92*, 5405.
(53) Duschinsky, F. *Acta Physicochim. URSS* **1937**, *7*, 551.
(54) Chen, P.; Logan, C. F.; and co-workers. FCF, CDECK Fortran programs, 1993.
(55) Ervin, K. M. *PESCAL*; Fortran program, 2001.
(56) Botter, R.; Dibeler, V. H.; Walker, J. A.; Rosenstock, H. M. *J. Chem. Phys.* **1966**, *44*, 1271.
(57) Beyer, T. S.; Swinehart, D. F. *Commun. ACM* **1973**, *16*, 379.
(58) Crawford, T. D.; Stanton, J. F.; Allen, W. D.; Schaefer, H. F., III. *J. Chem. Phys.* **1997**, *107*, 10626.
(59) Meot-Ner (Mautner), M.; Kafafi, S. A. *J. Am. Chem. Soc.* **1988**, *110*, 6297.
(60) Ruscic, B.; Feller, D.; Dixon, D. A.; Peterson, K. A.; Harding, L. B.; Asher, R. L.; Wagner, A. F. *J. Phys. Chem. A* **2001**, *105*, 1.
(61) DeTuri, V. F.; Ervin, K. M. *J. Phys. Chem. A* **1999**, *103*, 6911.
(62) Gurvich, L. V.; Veyts, I. V.; Alcock, C. B. *Thermodynamic Properties of Individual Substances*, 4th ed.; Hemisphere Publishing Corporation: New York, 1989; Vol. 1 (Elements O, H (D, T), F, Cl, Br, I, He, Ne, Ar, Kr, Xe, Rn, S, N, P, and Their Compounds), Parts 1−2.
(63) Gurvich, L. V.; Veyts, I. V.; Alcock, C. B. *Thermodynamic Properties of Individual Substances*, 4th ed.; Hemisphere: New York, 1991; Vol. 2 (Elements C, Si, Ge, Sn, Pb, and Their Compounds), Parts 1−2.
(64) Irikura, K. K. In *Computational Thermochemistry. Prediction and Estimation of Molecular Thermodynamics*; Irikura, K. K., Frurip, D. J., Eds.; American Chemical Society: Washington, DC, 1998; p 402.
(65) Taylor, B. N.; Kuyatt, C. *Guidelines for Evaluating and Expressing the Uncertainty of NIST Measurement Results*; NIST Technical Note 1297; National Institute of Standards and Technology: Washington, DC, 1994. (http://physics.nist/gov/Document/tn1297.pdf).
(66) Hare, M.; Emrick, T.; Eaton, P. E.; Kass, S. R. *J. Am. Chem. Soc.* **1997**, *119*, 237.
(67) Chase, M. W., Jr. *J. Phys. Chem. Ref. Data* **1998** (Monograph No. 9).
(68) Smith, J. R.; Kim, J. B.; Lineberger, W. C. *Phys. Rev. A* **1997**, *55*, 2036.
(69) Ruscic, B. Personal communication, 2001.
(70) Mordaunt, D. H.; Ashfold, M. N. R.; Dixon, R. N. *J. Chem. Phys.* **1996**, *104*, 6460.